Spectrochimica Acta Part A: Molecular and Biomolecular Spectroscopy 279 (2022) 121436

Contents lists available at ScienceDirect

Spectrochimica Acta Part A: Molecular and Biomolecular Spectroscopy

journal homepage: www.journals.elsevier.com/spectrochimica-acta-part-a-molecular-and-biomolecular-spectroscopy

Pressure- and temperature-dependent Raman spectra of $Ca_2Fe_2O_5$ oxygen defect perovskite

Shuangmeng Zhai [a,*], Bo Dai [a,b], Weihong Xue [a], Justin D. Rumney [c], Hu Wang [d], Sean R. Shieh [c], Xiang Wu [d]

[a] Key Laboratory of High-temperature and High-pressure Study of the Earth's Interior, Institute of Geochemistry, Chinese Academy of Sciences, Guiyang 550081, China
[b] University of Chinese Academy of Sciences, Beijing 100049, China
[c] Department of Earth Sciences, University of Western Ontario, London N6A 5B7, Canada
[d] State Key Laboratory of Geological Processes and Mineral Resources, China University of Geosciences, Wuhan 430074, China

ARTICLE INFO

Keywords:
$Ca_2Fe_2O_5$
Raman spectra
High pressure
High temperature
Phase transition

ABSTRACT

The Raman spectra of $Ca_2Fe_2O_5$ were investigated up to 21.8 GPa at room temperature and up to 1073 K at ambient pressure, respectively. A phase transition begins around 13.6 GPa and it is reversible after decompression. No temperature-induced phase transition was observed due to the quality of Raman spectra at temperatures above 773 K. The effects of pressure and temperature on the Raman vibration were quantitatively analyzed. All the observed Raman active vibrations of $Ca_2Fe_2O_5$ show positive linear pressure dependences and negative temperature dependences with different slopes. Combined with previous experimental results, the isothermal and isobaric mode Grüneisen parameters of $Ca_2Fe_2O_5$ were estimated, and the intrinsic anharmonicity was discussed.

1. Introduction

Perovskite, general formula as $A^{2+}B^{4+}X_3$, where A and B are cations and X is an anion, forms a very important class of inorganic crystals whose physical properties are extensively used in many technological applications [1]. Due to its broad applications and importance, a great number of perovskites have been widely investigated in past decades. Substitutions of quadrivalent ion by trivalent ions on the B coordination sites of perovskite introduce oxygen vacancies [2], i.e., $2B_B^{4+} = 2\,M_B^{3+} + V_{\ddot{O}}$, anion-deficient perovskite can thus be formed [3]. In $CaSiO_3$ perovskite, the Si^{4+} ions can be substituted by trivalent cations, such as Fe^{3+}, i.e., $2Si^{4+} = 2Fe^{3+} + V_{\ddot{O}}$, to form $Ca_2Fe_2O_5$ oxygen defect perovskite. $Ca_2Fe_2O_5$, a non-stoichiometric oxygen defect perovskite belonging to brownmillerite-subgroup [3], was naturally found and named as srebrodolskite [4]. $Ca_2Fe_2O_5$ srebrodolskite with space group *Pnma* consists of two main building units: layers of perovskite-type corner-sharing [FeO_6] octahedra and single chains of [FeO_4] tetrahedra [5–6], as shown in Fig. 1.

The physical and chemical properties of $Ca_2Fe_2O_5$ have been investigated in previous studies [7–16]. High-pressure in-situ X-ray diffraction measurements show that the compressibility of $Ca_2Fe_2O_5$ is largely lower than that of $CaSiO_3$ perovskite, indicating an elastic softening caused by vacancies on the oxygen positions [7–8]. High-temperature differential thermal analysis, neutron and X-ray diffraction studies of $Ca_2Fe_2O_5$ show a temperature-induced phase transition to space group *Ibm2* around 700 °C and the temperature dependence of lattice parameters were also estimated [9–16].

In previous studies, the Raman spectrum of $Ca_2Fe_2O_5$ has been reported at ambient conditions [17–19]. However, no available high-pressure or high-temperature Raman spectra of $Ca_2Fe_2O_5$ were reported to date. Furthermore, no phase transition was observed in previous high-pressure X-ray diffraction measurements since those studies were carried out at pressures less than 10 GPa [7–8]. In fact, pressure-induced phase transitions were observed in other brownmillerites including Ca_2AlFeO_5 and $Sr_2Fe_2O_5$ at higher pressures [20–21]. In this paper, we report the micro-Raman spectra of $Ca_2Fe_2O_5$ at pressures up to 21.8 GPa at room temperature and up to 1073 K at ambient pressure, respectively. A reversible pressure-induced phase transition was observed at 13.6 GPa. The pressure- and temperature-dependent Raman active modes of $Ca_2Fe_2O_5$ were quantitatively analyzed. Combined with previous results, the isothermal and isobaric mode Grüneisen parameters of $Ca_2Fe_2O_5$ were determined, and the intrinsic anharmonicity was

* Corresponding author.
E-mail address: zhaishuangmeng@mail.gyig.ac.cn (S. Zhai).

https://doi.org/10.1016/j.saa.2022.121436
Received 24 March 2022; Received in revised form 24 May 2022; Accepted 25 May 2022
Available online 28 May 2022

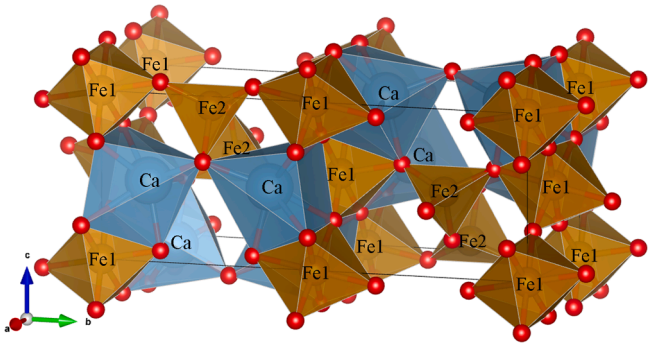

Fig. 1. The crystal structure of $Ca_2Fe_2O_5$.

estimated.

2. Experimental

Single phase $Ca_2Fe_2O_5$ srebrodolskite was synthesized by high-temperature solid state reaction method, similar to previous studies [9–10,13–15]. A mixture containing an appropriate ratio of reagent-grade $CaCO_3$ and Fe_2O_3 (99.99% purity) in a proportion corresponding to the $Ca_2Fe_2O_5$ was sufficiently ground then heated to 1523 K and kept for 48 h in furnace. The obtained sample was characterized by the PAN analytical's Empyrean X-ray diffractometer with monochromated CuKa radiation ($\lambda = 1.54056$ Å), operated at 40 kV and 45 mA. The powder X-ray diffraction pattern of the synthetic product indicates that the obtained sample was pure $Ca_2Fe_2O_5$ phase. A refinement gives lattice parameters as $a = 5.435(1)$ Å, $b = 14.814(1)$ Å, $c = 5.597(1)$ Å and $V = 450.7(1)$ Å^3, which are consistent with previous studies [9,11–12,14]. The ^{57}Fe-Mössbauer spectrum of synthetic sample was recorded with an OXFORD-MS500 spectrometer using a 50 mCi ^{57}CO/Pd radioactive source at room temperature in an ordinary mode. The measured Mössbauer spectrum including two sextets corresponding to magnetically octahedral and tetrahedral Fe^{3+}, is consistent with previous reports [22–24] and the relative areas of the two sextets are equal within experimental error. This indicates the equal amount of tetrahedral and octahedral sites in the crystal structure.

High-pressure Raman spectra were measured by using a symmetric type diamond anvils cell (DAC). The method and procedure is same as our previous study [20]. The synthetic $Ca_2Fe_2O_5$ sample was placed inside a rhenium gasket with a sample chamber of 120 μm in diameter, with neon as the pressure medium. Tiny ruby spheres as pressure marker were also loaded into the sample chamber. The experimental pressures were calculated by the ruby fluorescence method [25]. Raman spectra were collected by a custom-built Raman system equipped with a monochromatic Ar ion laser and a charge coupled device (CCD) detector cooled with liquid nitrogen at the University of Western Ontario [26]. Raman signals were excited by a 514.5 nm monochromatic argon ion beam and recorded by the CCD detector with a 0.5-meter focal length of collimator. The precision in the frequency determination of this micro-Raman system was about 1 cm^{-1}. The duration for each spectrum was 180 s, and the final spectrum was the average of five spectra collected at each pressure. The Raman shift of each band was obtained by Lorentzian curve fitting to get a reasonable approximation by using PeakFit program (SPSS Inc., Chicago).

Small pieces of $Ca_2Fe_2O_5$ sample were used for Raman spectroscopic measurements at various temperatures. The method and procedure is same as our previous studies [27–29]. Raman spectrometer (Horiba LabRam HR Evolution) equipped with an air-cooled CCD detector operating at 213 K and an 1800 gr/mm grating was used to collect over the frequency range from 200 to 800 cm^{-1}. The resolution of the Raman spectroscopy was 1 cm^{-1} in the measured frequency region. An argon-ion laser was used as exciting source and a power of 20 mW at the sample. An SLM Plan 20 × Olympus microscope objective was used to focus the laser beam and collect the scattered light. A sintered polycrystalline $Ca_2Fe_2O_5$ sample with dimensions of about 150 × 100 × 80 μm was put on a sapphire or silica window for high-temperature or low-temperature Raman spectroscopic measurements, respectively. The sapphire window was put into an alumina chamber in a Linkam TS 1500 for heating, while the silica window was placed at the center of a small silver block for freezing runs using THMSG 600. In high-temperature measurements, a resistance heater was used along with a water cooling system and an S-type thermocouple was used. In low-temperature measurements liquid nitrogen was pumped through an annulus in the silver block and a resistance heater opposes the cooling effect of the nitrogen to yield the desired temperature. In both modes, the temperature control unit is completely automatic and can be programmed to maintain at desired temperatures or to change temperature at a constant rate of 10 K/min. The measurement system has been calibrated at both high and low temperatures by observing phase changes in synthetic fluid inclusions placed in the center of the crucible. Horizontal thermal gradients may have errors of up to 1% in temperature measurements. The accumulation time for each spectrum was 60 s, and the final spectrum was the average of three collections. The Raman shift of each band was obtained by Lorentzian curve fitting using the PeakFit program (SPSS Inc., Chicago) to get a reasonable approximation.

3. Results and discussion

According to the factor group analysis of *Pnma* space group and general point group *D*2h (mmm) [30], the $Ca_2Fe_2O_5$ structure yields the following Raman active vibrations [17]:

$$\Gamma = 13A_g + 11B_{1g} + 13B_{2g} + 11B_{3g}.$$

Therefore, totally 48 Raman vibrational modes are predicted. However, the observed Raman bands are much less than those of predicted modes. It is due to some undetected weak Raman active modes and/or overlapping, and another reason is the limited wavenumber range (200–800 cm^{-1}).

3.1. Raman spectra under high pressures

Fig. 2(a) shows the typical Raman spectra of $Ca_2Fe_2O_5$ at different pressures. The Raman spectrum collected at 0.3 GPa shows seven peaks at and 264, 294, 317, 383, 431, 567 and 708 cm^{-1}, which are comparable with previous reported bands at ambient conditions [17–19]. These bands were assigned as A_g modes and attributed to internal vibrations of the FeO_6 octahedra [17–19]. Further, the bands at 264, 294, 317, 383 and 431 cm^{-1} are attributed to the rotation of the FeO_6 octahedra, the vibrational modes at 567 and 708 cm^{-1} are associated with the symmetric breathing and stretching of the FeO_6 octahedra [19,31]. It is noted that the Raman spectra of $Ca_2Fe_2O_5$ gradually shift to higher wavenumbers with increasing pressures. It is reasonable because the chemical bonds become shorter due to compression with increasing pressure and shorter bonds imply larger bond force constant, and consequently higher vibrational wavenumber according to the expression: $\upsilon = \frac{1}{2\pi c}\sqrt{\frac{f}{\mu}}$, where υ is vibrational wavenumber in cm^{-1}, c is velocity of light, f is force constant, and μ is the reduced mass of the mode (for diatomic molecule $1/\mu = 1/m_1 + 1/m_2$, for polyatomic molecules $1/\mu = \sum \frac{1}{m_i}$, where m_i is the mass of atom). Some bands become weak during compression and news peaks appear at 13.6 GPa, as indexed by arrows in Fig. 2(a). With further compression, the relative intensities of these new peaks become stronger and the typical bands of initial $Ca_2Fe_2O_5$ weaken and disappear. It indicates that a pressure-induced phase transition occurs during compression. The Raman spectrum collected after decompression to ambient pressure is same as the initial $Ca_2Fe_2O_5$, which means the pressure-induced phase transition is

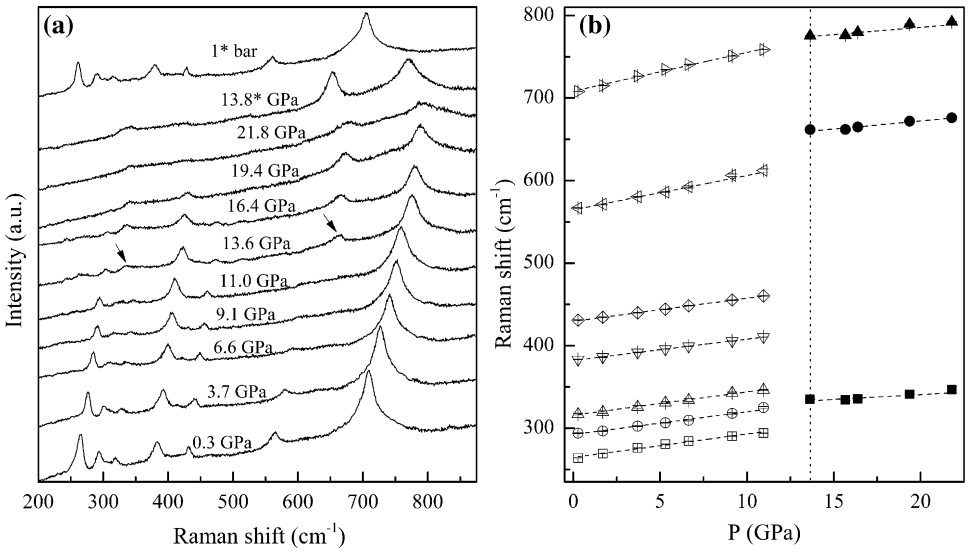

Fig. 2. (a) Typical Raman spectra of $Ca_2Fe_2O_5$ at various pressures and room temperature. The arrows index the appearance of new Raman peaks, and the Raman spectra at pressures with asterisk were collected during decompression. (b) The Raman shifts of vibrational modes in $Ca_2Fe_2O_5$ at various pressures and room temperature.

reversible. Actually, our observed Raman bands of $Ca_2Fe_2O_5$ at ambient conditions are in good agreement with the previous report of Piovano et al. [17]. These modes can be assigned to stretching vibrations with frequency >550 cm^{-1} and deformation mode with frequency between 250 and 550 cm^{-1}. The high-pressure phase of $Ca_2Fe_2O_5$ shows three Raman active bands, as illustrated in Fig. 2, and two stretching modes with frequency >550 cm^{-1} and one deformation mode with frequency between 250 and 550 cm^{-1} might be similarly assigned.

In previous high-pressure single-crystal X-ray diffraction studies on $Ca_2Fe_2O_5$ [7–8], no pressure-induced phase transition was observed since the pressure is not enough high (less than 10 GPa). As mentioned above, pressure-induced phase transitions were observed on Ca_2AlFeO_5 and $Sr_2Fe_2O_5$ at higher pressures [20–21]. Both Ca_2AlFeO_5 and $Sr_2Fe_2O_5$ are typical oxygen-deficient perovskites and in the space group of *Ibm2* at ambient conditions, whereas $Ca_2Fe_2O_5$ is in the space group of *Pnma*. High pressure X-ray diffraction and Raman spectroscopic study showed that Ca_2AlFeO_5 undergoes a reversible phase transition at around 26.5 GPa at room temperature [20]. Previous experimental and theoretical study indicated that brownmillerite $Sr_2Fe_2O_5$ transforms into a tetragonal perovskite-type phase (*I4/mcm*, Z = 4) at 12.0 GPa and room temperature, and then into a $Sr_2Mn_2O_5$-type phase (*Pbam*, Z = 2) at 23.3 GPa after high-temperature annealing [21]. The transition mechanism from brownmillerite $Sr_2Fe_2O_5$ to the tetragonal perovskite-type phase is suggested as the displacement of four-coordinated Fe^{3+} cations to higher coordinated positions upon compression [21]. Based on the present Raman spectroscopic measurements, the mechanism for the pressure-induced phase transition of $Ca_2Fe_2O_5$ and the structure of high-pressure phase cannot be deduced though it might relate to the evolution of [FeO_4] tetrahedra in $Ca_2Fe_2O_5$ during compression. Further study is required to verify the transition mechanism and structure of high-pressure form of $Ca_2Fe_2O_5$.

The effect of pressure on the Raman shift of is illustrated in Fig. 2(b). Seven Raman active bands were distinguished for $Ca_2Fe_2O_5$ srebrodolskite and three bands for high-pressure form of $Ca_2Fe_2O_5$ in the range of 200–800 cm^{-1}. The pressure coefficients (b_{iP}) for different bands are listed in Table 1. All the pressure coefficients are positive, indicating the Raman shifts of vibrations in $Ca_2Fe_2O_5$ increase with pressure. Obviously, the pressure coefficients of high-frequency vibrations (4.14–4.69 cm^{-1}/GPa) are larger than those of low-frequency vibrations (2.58–2.83 cm^{-1}/GPa) in $Ca_2Fe_2O_5$ srebrodolskite. On the other hand, the pressure coefficients for vibrations of $Ca_2Fe_2O_5$ srebrodolskite (2.58–4.69 cm^{-1}/GPa) are different from those of high-pressure form of $Ca_2Fe_2O_5$ (1.19–1.94 cm^{-1}/GPa). The discontinuous changes of the pressure coefficients also indicate a pressure-induced phase transition of $Ca_2Fe_2O_5$ oxygen defect perovskite. Different pressure coefficients means the effect of pressure on the Raman vibrations are various, which is related to the different evolutions of chemical bonds under compression.

Table 1
The parameters of linear dependence on pressure $\nu_{iP} = a_{iP} + b_{iP} P$ at room temperature and on temperature $\nu_{iT} = a_{iT} + b_{iT} T$ at ambient pressure, the isothermal and isobaric mode Grüneisen parameter (γ_{iT} and γ_{iP}), and the intrinsic anharmonic mode parameter, β_i, for $Ca_2Fe_2O_5$.

Raman no.	a_{iP}	b_{iP}	γ_{iT}	a_{iT}	$-b_{iT} \times 10^2$	γ_{iP}	$\beta_i \times 10^5$
1	258.7 (8)	2.83 (14)	1.40	261.1 (9)	1.61 (14)	1.55	−0.60
2	289.1 (5)	2.73 (12)	1.21	292.3 (8)	1.23 (15)	1.05	0.64
3	314.0 (5)	2.82 (6)	1.15	316.2 (8)	0.86 (13)	0.68	1.88
4	380.1 (1)	2.58 (2)	0.87	382.1 (9)	0.92 (14)	0.60	1.08
5	429.5 (2)	2.80 (3)	0.83	434.0 (9)	2.37 (15)	1.37	−2.15
6	560.3 (7)	4.14 (16)	0.95	565.2 (7)	2.52 (20)	1.12	−0.68
7	708.4 (10)	4.69 (14)	0.85	712.7 (6)	1.75 (11)	0.62	0.92
1*	316.9 (12)	1.19 (20)					
2*	633.4 (15)	1.94 (18)					
3*	750.9 (18)	1.74 (23)					

ν_{iP}, ν_{iP}, a_{iP} and a_{iT} in cm^{-1}, P in GPa, b_{iP} in cm^{-1} GPa^{-1}, T in K, b_{iT} in cm^{-1} K^{-1}, and β_i in K^{-1}. The Raman nos. with * are of high-pressure phase.

3.2. Raman spectra at various temperatures

The typical Raman spectra of $Ca_2Fe_2O_5$ at different temperatures are illustrated in Fig. 3(a). It is obvious that the Raman spectra of $Ca_2Fe_2O_5$ gradually shift to lower wavenumbers with increasing temperatures. It is reasonable because the Fe-O bonds become longer due to expansion

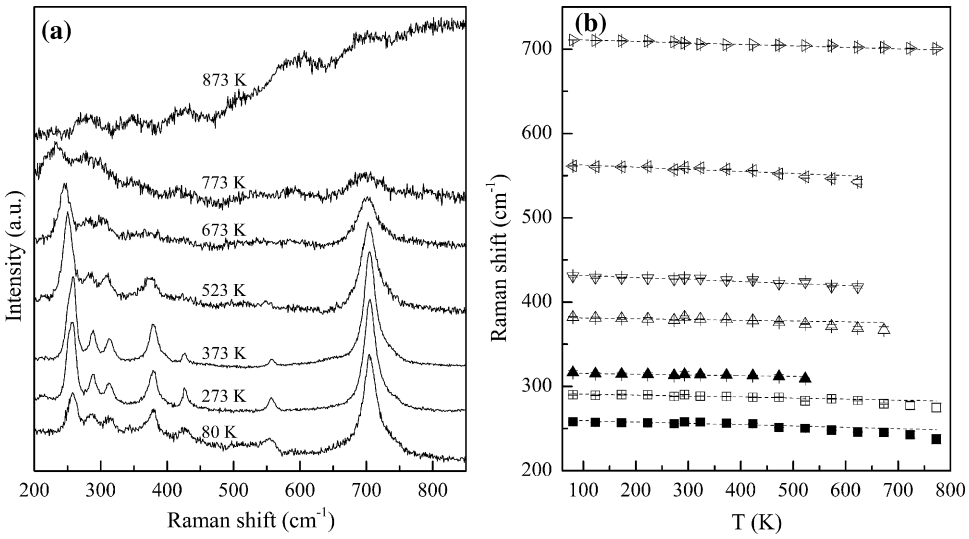

Fig. 3. (a) Typical Raman spectra of $Ca_2Fe_2O_5$ at different temperatures and ambient pressure. (b) The Raman shifts of vibrational modes in $Ca_2Fe_2O_5$ at different temperatures and ambient pressure.

with increasing temperature and longer bonds imply smaller bond force constant, and consequently lower vibrational wavenumber according to the above mentioned expression: $\upsilon = \frac{1}{2\pi c}\sqrt{\frac{f}{\mu}}$. Some vibrational modes become weak and disappear during heating.

In previous studies of $Ca_2Fe_2O_5$ by high-temperature differential thermal analysis, neutron and X-ray diffraction measurements [9–16], a temperature-induced phase transition from space group *Pnma* to *Ibm2* was reported around 700 °C. In the present high-temperature Raman spectroscopic study, no phase transition was observed though the highest temperature was 1073 K. The reason is that the Raman signal becomes very weak and broad under higher temperature due to high background, as shown in Fig. 3(a). Therefore, it is impossible to distinguish the vibrations above 773 K.

The variation of Raman shift for $Ca_2Fe_2O_5$ at different temperatures is plotted in Fig. 3(b), which shows nearly linear relationships with different slopes for different modes. As listed in Table 1, the temperature coefficients (b_{iT}) of vibrational modes in $Ca_2Fe_2O_5$ show that the high-wavenumber modes are more sensitive to temperature compared to the low-wavenumber vibrations. In fact, the temperature coefficients of high-wavenumber modes in $Ca_2Fe_2O_5$ are -1.75 to -2.52×10^{-2} cm^{-1} K^{-1}, whereas the coefficients for low-wavenumber vibrations are -0.86 to -1.61×10^{-2} cm^{-1} K^{-1}.

3.3. Mode Grüneisen parameters and anharmonicity

The Grüneisen parameter is of great importance for the thermal equation of state of materials at high pressures [32]. The variations of the different Raman vibrations under pressures and temperatures can be used to obtain the isothermal and isobaric mode Grüneisen parameter, γ_{iT} and γ_{iP}, based on the following expressions [33–34]:

$$\gamma_{iT} = K_T(\ln\nu_{iP}/P)_T$$

$$\gamma_{iP} = -1/\alpha(\ln\nu_{iT}/T)_P$$

where K_T is the isothermal bulk modulus, α is the thermal expansion coefficient, ν_{iP} and ν_{iT} are the vibrational wavenumbers of the i^{th} mode under pressures and temperatures. The isothermal bulk modulus of $Ca_2Fe_2O_5$ was reported as 127.0 GPa [7] and 128.0 GPa [8]. The thermal expansion coefficient α of $Ca_2Fe_2O_5$ was previously reported in different studies, as summarized in Table 2. It is noted that different studies yield discrepant thermal expansion coefficients. By adopting K_T of 128.0 GPa [8] and α of 3.99×10^{-5} K^{-1} [15], the calculated values of γ_{iT} and γ_{iP} for different vibrational modes of $Ca_2Fe_2O_5$ are also listed in Table 1. The isothermal and isobaric mode Grüneisen parameter (γ_{iT} and γ_{iP}) are in the ranges of 0.83–1.40 and 0.60–1.55.

Table 2
Thermal expansion coefficients ($\times 10^{-5}$ K^{-1}) of $Ca_2Fe_2O_5$.

a	α_a	a_b	α_c	Sample state	Method	Ref.
3.76 (8)	1.01 (3)	1.79 (2)	0.96 (2)	Powder	Neutron diffraction	[9]
4.13	0.88	2.31	0.93	Powder	X-ray diffraction	[11]
4.08	1.03	2.19	0.83	Powder	X-ray diffraction	[12]
3.99 (6)	0.98 (3)	2.19 (3)	0.81 (3)	Powder	X-ray diffraction	[15]
4.11 (9)	1.08 (1)	1.47 (1)	1.57 (3)	Single crystal	Dilatometry	[16]

α_a, α_b, and α_c represent the axial thermal expansion coefficients along *a*-, *b*- and *c*-axis, respectively.

The intrinsic anharmonic mode parameter, βi, also can be calculated using the obtained isothermal and isobaric mode Grüneisen parameter (γ_{iT} and γ_{iP}) as follow [33–34]:

$$\beta i = \alpha(\gamma_{iT} - \gamma_{iP}).$$

Similarly, the thermal expansion coefficient α of 3.99×10^{-5} K^{-1} for $Ca_2Fe_2O_5$ [15] was used to calculate βi, and the results are also listed in Table 1. It is noted that the values of β_i are non-zero, indicating an intrinsic anharmonicity exists $Ca_2Fe_2O_5$.

4. Conclusions

By using Raman spectroscopic measurements, the stability and effect of pressure and temperature on vibrational modes in $Ca_2Fe_2O_5$ oxygen defect perovskite have been investigated up to 21.8 GPa at room temperature and up to 1073 K at ambient pressure, respectively. A reversible pressure-induced phase transition at 13.6 GPa in $Ca_2Fe_2O_5$ was observed. The Raman shifts of all observed vibrations for $Ca_2Fe_2O_5$ linearly increase with increasing pressure and decrease with increasing temperature in different slopes. The isothermal and isobaric mode Grüneisen parameters of $Ca_2Fe_2O_5$ were estimated at 0.83–1.40 and 0.60–1.55, respectively. The intrinsic anharmonic mode parameters of $Ca_2Fe_2O_5$ were estimated to be non-zero and in the range from -2.15×10^5 K^{-1} to 1.88×10^5 K^{-1}.

CRediT authorship contribution statement

Shuangmeng Zhai: Conceptualization, Writing – original draft, Funding acquisition. **Bo Dai:** Investigation. **Weihong Xue:** Investigation. **Justin D. Rumney:** Data curation. **Hu Wang:** Data curation. **Sean R. Shieh:** Methodology, Writing – review & editing, Funding acquisition. **Xiang Wu:** Methodology.

Declaration of Competing Interest

The authors declare that they have no known competing financial interests or personal relationships that could have appeared to influence the work reported in this paper.

Acknowledgements

The authors thank Dr. Nandita Maiti for the editorial handling and three anonymous referees for their constructive reviews. This study was financially supported by the National Natural Science Foundation of China (Grant No. U1532126), the Chinese Academy of Sciences (Grant No. 132852KYSB20200011) and the Natural Sciences and Engineering Research Council of Canada (RGPIN/06818-2019). The high-pressure Raman spectroscopic measurements were performed at University of Western Ontario, and the Raman spectra at various temperatures were collected at China University of Geosciences (Wuhan).

References

[1] R.H. Mitchell, Perovskites: modern and ancient, Almaz Press, Thunder Bay, 2002.
[2] A. Navrotsky, A lesson from Ceramics, Science 284 (5421) (1999) 1788–1789.
[3] M.W. Lufaso, P.M. Woodward, Prediction of the crystal structures of perovskites using the software program SPuDS, Acta Crystallogr. B 57 (6) (2001) 725–738.
[4] B.V. Chesnokov, L.F. Bazhenova, Srebrodolskite $Ca_2Fe_2O_5$ – a new mineral, Zap. Vses. Mineral. Obshch. 114 (1985) 195–199.
[5] A.A. Colville, The crystal structure of $Ca_2Fe_2O_5$ and its relations to the nuclear elec tric field gradient at the iron sites, Acta Crystallogr. B 26 (1970) 1469–1473.
[6] J. Berggren, Refinement of the crystal structure of dicalcium ferrite, $Ca_2Fe_2O_5$, Acta Chem. Scand. 25 (1971) 3616–3624.
[7] N.L. Ross, R.J. Angel, F. Seifert, Compressibility of brownmillerite ($Ca_2Fe_2O_5$): effect of vacancies on the elastic properties of perovskites, Phys. Earth Planet. Inter. 129 (1-2) (2002) 145–151.
[8] C.B. Vanpeteghem, R.J. Angel, J. Zhao, N.L. Ross, G.J. Redhammer, F. Seifert, The effect of oxygen vacancies and aluminium substitution on the high-pressure properties of brownmillerite-structured $Ca_2Fe_{2-x}Al_xO_5$, Phys. Chem. Miner. 35 (9) (2008) 493–504.
[9] P. Berastegui, S.-G. Eriksson, S. Hull, A neutron diffraction study of the temperature dependence of $Ca_2Fe_2O_5$, Mater. Res. Bull. 34 (2) (1999) 303–314.
[10] K. Fukuda, H. Ando, Determination of the *Pcmn/Ibm2* phase boundary at high temperatures in the system $Ca_2Fe_2O_5$-$Ca_2Al_2O_5$, J. Am. Ceram. Soc. 85 (2002) 1300–1302.
[11] G.J. Redhammer, G. Tippelt, G. Roth, G. Amthauer, Structural variations in the brownmillerite series $Ca_2(Fe_{2-x}Al_x)O_5$: Single-crystal X-ray diffraction at 25 °C and high-temperature X-ray powder diffraction (25 °C ≤ T ≤ 1000 °C), Am. Mineral. 89 (2004) 405–420.
[12] A. Shaula, Y. Pivak, J. Waerenborgh, P. Gaczynski, A. Yaremchenko, V. Kharton, Ionic conductivity of brownmillerite-type calcium ferrite under oxidizing conditions, Solid State Ionics 177 (33-34) (2006) 2923–2930.
[13] H. Krüger, V. Kahlenberg, V. Petříček, F. Phillipp, W. Wertl, High-temperature structural phase transition in $Ca_2Fe_2O_5$ studied by in-situ X-ray diffraction and transmission electron microscopy, J. Solid State Chem. 182 (2009) 1515–1523.
[14] E. Asenath-Smith, I.N. Lokuhewa, S.T. Misture, D.D. Edwards, p-Type thermoelectric properties of the oxygen-deficient perovskite $Ca_2Fe_2O_5$ in the brownmillerite structure, J. Solid State Chem. 183 (2010) 1670–1677.
[15] E. Asenath-Smith, S.T. Misture, D.D. Edwards, Structural behavior and thermoelectric properties of the brownmillerite system $Ca_2(Zn_xFe_{2-x})O_5$, J. Solid State Chem. 184 (8) (2011) 2167–2177.
[16] T. Labii, M. Ceretti, A. Boubertakh, W. Paulus, S. Hamamda, Dilatometric study of $CaFeO_{2.5}$ single crystal, J. Therm. Anal. Calorim. 112 (2013) 865–870.
[17] A. Piovano, M. Ceretti, M.R. Johnson, G. Agostini, W. Paulus, C. Lamberti, (2015). Anisotropy in the Raman scattering of a $CaFeO_{2.5}$ single crystal and its link with oxygen ordering in Brownmillerite frameworks, J. Phys-Condens. Mat. 27 (2015) 225403.
[18] S. Dhankhar, G. Bhalerao, S. Ganesamoorthy, K. Baskar, S. Singh, Growth and comparison of single crystals and polycrystalline brownmillerite $Ca_2Fe_2O_5$, J. Cryst. Growth 468 (2017) 311–315.
[19] T.-L. Phan, N. Tran, D.H. Kim, P.T. Tho, B.T. Huy, T.N. Dang, D.-S. Yang, B. Lee, Electronic structure and magnetic properties of Al-doped $Ca_2Fe_2O_5$ brownmillerite compounds, J. Am. Ceram. Soc. 101 (5) (2018) 2181–2189.
[20] Z. Li, Y. Yin, J.D. Rumney, S.R. Shieh, J. Xu, D. Fan, W. Liang, S. Yan, S. Zhai, High-pressure in-situ X-ray diffraction and Raman spectroscopy of Ca_2AlFeO_5 brownmillerite, High Pressure Res. 39 (1) (2019) 92–105.
[21] F. Zhu, Y.e. Wu, X. Lai, S. Qin, K.e. Yang, J. Liu, X. Wu, Experimental and theoretical investigations on high-pressure phase transition of $Sr_2Fe_2O_5$, Phys. Chem. Miner. 41 (6) (2014) 449–459.
[22] H.J. Whitfield, Mössbauer effect in the system $Ca_2Fe_2O_5$-Ca_2FeAlO_5, Aust. J. Chem. 20 (1967) 859–867.
[23] A.I. Becerro, F. Langenhorst, R.J. Angel, S. Marion, C.A. McCammon, F. Seifert, The transition from short-range to long-range ordering of oxygen vacancies in $CaFe_xTi_{1-x}O_{3-x/2}$ perovskites, Phys. Chem. Chem. Phys. 2 (2000) 3933–3941.
[24] G.J. Redhammer, G. Amthauer, G. Tippelt, W. Lottermoser, G. Roth, ^{57}Fe Mössbauer spectroscopic investigations on the brownmillerite series $Ca_2(Fe_{2-x}Al_x)O_5$, AIP Conf. Proc. 765 (2005) 179–184.
[25] H.K. Mao, J. Xu, P.M. Bell, Calibration of the ruby pressure gauge to 800 kbar under quasi-hydrostatic conditions, J. Geophys. Res. Solid Earth 91 (1986) 4673–4767.
[26] W. Yong, S. Botis, S.R. Shieh, W. Shi, A.C. Withers, Pressure-induced phase transition study of magnesiochromite ($MgCr_2O_4$) by Raman spectroscopy and X-ray diffraction, Phys. Earth Plane. Inter. 196–197 (2012) 75–82.
[27] S. Zhai, K. Zhai, H. Wang, X. Wu, W. Xue, Temperature-induced phase transition of $Ca_2AlSiO_{5.5}$: Raman spectroscopic study, Vib. Spectrosc. 103 (2019), 102935.
[28] X. Hu, K. Zhai, M. Jia, Y. Liu, X. Wu, W. Wen, W. Xue, S. Zhai, Phase transition of $Mg_3(PO_4)_2$ polymorphs at high-temperature: In-situ synchrotron X-ray diffraction and Raman spectroscopic study, Spectrochim. Acta A. 269 (2022), 120762.
[29] W. Xue, K. Zhai, X. Wang, W. Wu, S.Z. Wen, Raman spectroscopic and X-ray diffraction study of α- and β-$Mg_2P_2O_7$ at various temperatures, Spectrochim. Acta A. 273 (2022), 121076.
[30] M.I. Aroyo, A. Kirov, C. Capillas, J.M. Perez-Mato, H. Wondratschek, Bilbao Crystallographic Server. II. Representations of crystallographic point groups and space groups, Acta Crystallogr. A 62 (2) (2006) 115–128.
[31] B. Lazic, H. Krüger, V. Kahlenberg, J. Konzett, R. Kaindl, Incommensurate structure of $Ca_2Al_2O_5$ at high temperatures – structure investigation and Raman spectroscopy, Acta Crystallogr. B 64 (4) (2008) 417–425.
[32] R. Boehler, J. Ramakrishnan, Experimental results on the pressure dependence of the Grüneisen parameter: A review, J. Geophys. Res. Solid Earth 85 (1980) 6996–7002.
[33] P. Gillet, F. Guyot, J. Malezieux, High-pressure and high-temperature Raman spectroscopy of Ca_2GeO_4: some insights on anharmonicity, Phys. Earth Planet. Inter. 58 (1989) 141–154.
[34] T. Okada, T. Narita, T. Nagai, T. Yamanaka, Comparative Raman spectroscopic study on ilmenite-type $MgSiO_3$ (akimotoite), $MgGeO_3$, and $MgTiO_3$ (geikielite) at high temperatures and high pressures, Am. Mineral. 93 (1) (2008) 39–47.